Chemical Engineering Journal 143 (2008) 337–348

Contents lists available at ScienceDirect

Chemical Engineering Journal

journal homepage: www.elsevier.com/locate/cej

Preparation and characterization of a dye–ligand adsorbent for lysozyme adsorption

Cristina Garcia-Diego*, Jorge Cuellar

Department of Chemical Engineering, University of Salamanca, Plaza de los Caidos 1-5, 37008 Salamanca, Spain

ARTICLE INFO

Article history:
Received 18 March 2008
Received in revised form 30 May 2008
Accepted 13 June 2008

Keywords:
Macroreticular
poly(styrene-*co*-divinylbenzene)
microparticles
Functionalization
Pore size distribution
Lysozyme adsorption

ABSTRACT

Dye–ligand macroreticular poly(styrene-*co*-divinylbenzene) microparticles with different pore properties have been obtained and used as adsorbents of proteins. To do so, plain microparticles were first coated with poly(vinyl alcohol) to shield the hydrophobic polymer surface from non-specifically adsorbing protein. The poly(vinyl alcohol) coating was then chemically cross-linked with glutaraldehyde to obtain a stable layer. Following this, Cibacron Blue F3GA, which was chosen as the dye affinity ligand, was immobilized on these microparticles to obtain specific protein adsorption. After each modification step, the pore size distributions of the microparticles were determined, observing that the adsorption of poly(vinyl alcohol) clogged micropores and low-interval mesopores, and that only microparticles with a high pore volume, basically due to high-interval mesopores and macropores, largely continued to exhibit these pores. The batch adsorption properties of the functionalized microparticles were studied using lysozyme as a model protein, observing that the existence of high-interval mesopores and macropores was essential in the adsorption of the protein. In fact, it was only possible to evaluate the adsorption characteristics in the case of microparticles that largely continued to display this kind of pores after their functionalization. Adsorption equilibrium was found to be described well by the Sips model, with a maximum adsorption capacity of 100.8 mg g^{-1} dry adsorbent. With regard to adsorption kinetics, both pore-diffusion and solid-diffusion models were used to estimate the diffusion coefficients, with the observation that the simplified solid-diffusion model was reliable for describing the experimental kinetic data, with a diffusion coefficient of 1.4×10^{-9} cm^2 s^{-1}. The non-specific adsorption of lysozyme on the functionalized microparticles was found to be 2.6 mg g^{-1} dry adsorbent. Finally, regarding desorption of the protein, it was observed that more than 73% of the lysozyme adsorbed was readily desorbed in a desorption medium containing 1.0 mol L^{-1} NaCl at pH 7.3.

1. Introduction

Among all the mechanisms used in biomacromolecular separation processes, affinity chromatography is considered to be the most specific because it relies on the specificity of a ligand–biomacromolecule interaction [1]. Affinity systems have a broad range of applications, and they have been used in the isolation and purification of enzymes, hormone receptors, cancer cell-surface antigens, membrane proteins and interferons [2]. Moreover, it seems probable that in the future the range of applications will increase and that novel techniques based on bimolecular recognition will continue to be developed.

The basic requirements for the development of an affinity purification system are an inert matrix material, an affinity ligand, and coupling reagents that allow covalent attachment of the ligand to the matrix.

Use of the affinity chromatography technique has been limited by problems associated with the support matrix, especially when high pressures must be used during the separation process. Agarose, which is a low-charge fraction of seaweed polysaccharide agar, is the most widely used support matrix, but its lack of mechanical stability, even in heavily cross-linked varieties, restricts its application in large-scale operations [3]. In contrast, synthetic macroreticular polymers are increasingly being used – in particular, adsorbents based on poly(styrene-*co*-divinylbenzene) (poly[S-*co*-DVB]) – owing to their good mechanical and chemical properties, their versatility and their pore structure [3–6]. However, the use of poly[S-*co*-DVB] microparticles as adsorbents of proteins is subject to two types of problem: (a) they cannot be used directly to purify proteins because hydrophobic interactions between the polymeric matrix and protein often result in irreversible adsorption, and (b) their direct derivatization with affinity ligands is difficult. There-

* Corresponding author. Tel.: +34 923294479; fax: +34 923294574.
E-mail address: cristinagd@usal.es (C. Garcia-Diego).

1385-8947/$ – see front matter © 2008 Elsevier B.V. All rights reserved.
doi:10.1016/j.cej.2008.06.022

Nomenclature

A	coefficient in Eq. (6)
b	Langmuir equilibrium coefficient of the adsorption sites (mL mg^{-1})
c	concentration of Lys in the pores (mg mL^{-1})
$C_{e,Lys}$	concentration of Lys in the supernatant at equilibrium (mg mL^{-1})
C_i	concentration of the adsorbable in the supernatant (mg mL^{-1})
$C_{o,i}$	initial concentration of the adsorbable in the solution (mg mL^{-1})
D_e	effective pore diffusivity of Lys (cm^2 s^{-1})
D_s	solid diffusivity of Lys (cm^2 s^{-1})
H_0	null hypothesis
H_1	alternative hypothesis
I_1	parameter defined by Eq. (10)
I_2	parameter defined by Eq. (11)
n	term in Eq. (6)
n_{plain}	sample size for the plain S2 microparticles
$n_{with\ PVA}$	sample size for the PVA-coated S2 microparticles
p_n	non-zero roots of Eq. (17)
q'	Lys concentration in the particles on a pore-free basis (mg mL^{-1})
$\bar{q}^*$	particle-average Lys concentration at equilibrium (mg mL^{-1})
$q_{e,i}$	amount of Lys (or PVA) adsorbed at equilibrium on the particles (mg g^{-1})
q_i	amount of Lys (or PVA) adsorbed at different times on the particles (mg g^{-1})
q^*_m	maximum Lys adsorption capacity on the particles (mg mL^{-1})
q_m	maximum Lys adsorption capacity on the particles (mg g^{-1})
$q_{non\text{-}ads}$	amount of Lys non-specifically adsorbed at equilibrium on the particles (mg g^{-1})
r	radial position in the microparticles (cm)
R^2	coefficient of determination
R_p	average value of the particle radius (cm)
S_{BET}	BET specific surface area (m^2 g^{-1})
S^2_p	variance defined by Eq. (4)
S^2_{plain}	individual sample variance for the plain S2 microparticles
$S^2_{with\ PVA}$	individual sample variance for the PVA-coated S2 microparticles
t	uptake time (s); t-statistic
V	bulk solution volume (mL)
V_{ads}	volume of nitrogen adsorbed on the microparticles (cm^3 g^{-1} STP)
V_{micro}	volume of micropores (cm^3 g^{-1})
V_M	volume of microparticles (mL)
$V_{o,i}$	initial volume of adsorbable solution (mL)
ΔV_i	dilution due to the humidity of the adsorbent (mL)
W	dry-adsorbent weight (g)
$\bar{y}_{plain}$	sample mean of the pore property for the plain S2 microparticles
$\bar{y}_{with\ PVA}$	sample mean of the pore property for the PVA-coated S2 microparticles

Greek letters

α	significance level of the test
ε_p	intraparticle porosity of the adsorbent
η	parameter defined by Eq. (12)
λ	parameter defined by Eq. (14)
Λ	fractional amount of Lys ultimately taken up by the adsorbent, defined in Eq. (13)
μ_{plain}	mean pore property for the plain S2 microparticles
$\mu_{with\ PVA}$	mean pore property for the PVA-coated S2 microparticles
χ^2	chi-square value

fore, the modification of their surface to prevent hydrophobic interactions and the introduction of coupling reagents to overcome the second problem are crucial requirements for obtaining a support based on poly[S-*co*-DVB] suitable for their subsequent functionalization and use as affinity adsorbents. In this sense, research oriented to the modification of the surface of poly[S-*co*-DVB] matrices to mask their hydrophobic surface with hydrophilic groups has been carried out [3–12]. One of the methods used involves a hydrophilic coating of the surface, which can be attained by using a copolymer containing both hydrophobic and hydrophilic segments [8]. Thus, if a copolymer of this type is dissolved in a polar solvent and exposed to the poly[S-*co*-DVB] microparticles, hydrophobic segments of the copolymer will adsorb on their surface, while the hydrophilic segments will loop outwards away from the surface like filaments. With this procedure, it is expected that the hydrophobic character of poly[S-*co*-DVB] will be completely masked and that the surface of the copolymer-support composite will exhibit the properties of the hydrophilic segments. Owing to its high degree of functionality, poly(vinyl alcohol) (PVA) seems to be an appropriate copolymer for coating the poly[S-*co*-DVB] surface. However, since it has been demonstrated that PVA partially desorbs when exposed to protein solutions [6], it is usual to increase both the chemical and the mechanical strength of the adsorbed layer by cross-linking it. Several reagents can be used as cross-linkers [3–7], the one most widely used being glutaraldehyde.

With regard to the ligand to be immobilized, a broad array of functional molecules, such as proteins, enzymes, antibodies, amino acid derivatives, oligopeptides, and nucleic acids can be used as ligands. However, in most cases these ligands have certain problems: (a) they are usually expensive and extremely specific, (b) there are difficulties involved in immobilizing them without loss of their original biological activity, and (c) they may be unable to withstand harsh cleaning conditions during use. To overcome these problems, triazine dye ligands have been considered as important alternatives to natural counterparts for specific affinity chromatography [13]. These ligands are able to bind most types of proteins, especially enzymes, in some cases acting in a remarkably specific manner [14]. Among all of the triazine dyes, Cibacron Blue F3GA is one of the most widely preferred ligands in the dye-affinity separation of proteins [15,16].

Although dye-immobilized adsorbents have been extensively used for protein purification [17], we have not found any study covering from the synthesis of the macroreticular poly[S-*co*-DVB] microparticles to their use as affinity adsorbents that has addressed the equilibrium and kinetics of the adsorption, with the corresponding modelling. Thus, the aim of the present work was to carry out a global investigation into the production and application of this type of adsorbent, studying the results of each modification introduced into the plain microparticles and the implications of such modifications in the final result.

To attain this objective, two types of macroreticular poly[S-*co*-DVB] microparticles were synthesized from mixtures with different divinylbenzene and diluent concentrations according

to an experimental procedure described elsewhere [18]. These microparticles were first coated with PVA and then chemically cross-linked with glutaraldehyde. Finally, Cibacron Blue F3GA ligand was immobilized on the microparticles. Modification of their pore size distribution was also investigated. Additionally, the resulting functionalized adsorbents were characterized by protein uptake equilibrium and kinetic studies using lysozyme (Lys) as a model protein. The non-specific adsorption and desorption of Lys were also tested.

2. Experimental

2.1. Chemicals

Poly(vinyl alcohol) (with a weight-average molar mass of 13,000–23,000 and a degree of hydrolysis of 87–89%) and the cross-linking agent, in this case glutaraldehyde (50% in water), were obtained from Sigma–Aldrich (Madrid, Spain). Hydrochloric acid at 35%, used as the catalyst in the cross-linking step of the adsorbed PVA layer, was supplied by Scharlab (Barcelona, Spain). The reagents used in the functionalization of the modified matrices were Cibacron Blue F3GA, which was obtained from Fluka Biochemika (Madrid, Spain), and sodium chloride and anhydrous sodium carbonate, both of which were supplied by Scharlab (Barcelona, Spain). Other reagents such as 99.5% sodium azide (Sigma–Aldrich, Madrid, Spain), and methanol multisolvent and hydrogen sodium carbonate (both obtained from Scharlab, Barcelona, Spain), were used in the conditioning of the microparticles.

To check the usefulness of the hydrophilic microparticles as adsorbents of proteins, lysozyme from chicken egg white (Lys, lyophilized powder, 95% approximately, from Sigma–Aldrich, Madrid, Spain) was used as a model protein. Salt-phosphate buffer solutions were prepared from monobasic anhydrous sodium phosphate and dibasic anhydrous potassium phosphate (Panreac, Barcelona, Spain), and sodium chloride (Scharlab, Barcelona, Spain), all of them of reagent grade. All sample solutions were microfiltered through a 0.45-μm syringe membrane filter (Millex-HV, Millipore Iberica).

2.2. Experimental procedure

Two types of macroreticular poly(styrene-*co*-divinylbenzene) (poly[S-*co*-DVB]) microparticles (S1 and S2) synthesized under different operating conditions were used. They were synthesized at our laboratory by means of the suspension polymerization technique, using *n*-heptane as porogen, as described elsewhere [18]. Their synthesis conditions, together with their structural characteristics, are summarized in Table 1. Sample S1 proved to have good adsorption and structural properties, as well as good mechanical strength [18–20]. With respect to the S2 microparticles, these displayed enhanced adsorption properties as regards both adsorption equilibrium and adsorption diffusivity [20].

Table 1
Synthesis conditions of the plain macroreticular poly(styrene-*co*-divinylbenzene) microparticles

Property	Samples	
	S1	S2[a]
DVB concentration (wt%)[b]	55.0	42.5
Monomeric fraction (v/v)[c]	0.60	0.50
Mean particle size (μm)	170	170
BET specific surface area ($m^2\,g^{-1}$)	434	376
t-Plot micropore volume ($cm^3\,g^{-1}$)	0.06	0.05
Cumulative volume of pores between 10 Å and 1000 Å radius ($cm^3\,g^{-1}$)	0.81	0.97
Cumulative surface area of pores between 10 Å and 1000 Å radius ($m^2\,g^{-1}$)	372	340
Average pore radius (Å)	44	57
Modal pore radius (Å)	244	284

[a] Pore properties are the corresponding to the first replicate of plain S2 microparticles, because these are the microparticles used in the functionalization and adsorption experiments.
[b] DVB concentration is the weight percentage of DVB isomers in the monomeric mixture.
[c] The monomeric fraction in the organic phase is the volume fraction of the monomers in the organic phase.

2.2.1. Coating of the polystyrene matrix with PVA

Macroreticular poly[S-*co*-DVB] microparticles were first washed extensively with methanol and then with deionized water. Following this, the microparticles were equilibrated overnight with water, which was later removed. The dry-weight fraction of the wet microparticles, *W* (g), was determined from the weight loss of the samples after 24 h in an oven at 110 °C.

After washing, 15.0 g of wet polymeric microparticles were placed in a round-bottomed flask and 250 mL of PVA solution was added at an initial concentration of 50 mg mL^{-1}. The solution was heated to 30 °C and stirred mechanically at 50 rpm for 3 days. To determine the PVA adsorption kinetics, samples of supernatant were removed on a regular basis to measure the concentration of PVA (C_{PVA}, expressed in units of mg mL^{-1}) with a UV–Vis spectrophotometer (Varian, model Cary 50) at 320 nm. The amount of PVA adsorbed per unit dry weight of adsorbent (q_{PVA}, mg g^{-1} of dry adsorbent) was obtained from the mass balance:

$$q_i = \frac{V_{o,i}C_{o,i} - (V_{o,i} + \Delta V_i)C_i}{W} \quad (1)$$

where q_i is the amount of adsorbate which is adsorbed on the adsorbent (mg g^{-1}); $V_{o,i}$ is the initial volume of the solution (mL); ΔV_i represents the dilution due to the humidity of the adsorbent (mL); $C_{o,i}$ is the initial concentration of the adsorbable in the solution (mg mL^{-1}); C_i is the concentration at time *t* (mg mL^{-1}); *W* is the dry-adsorbent weight (g).

The PVA-coated poly[S-*co*-DVB] microparticles were then washed thoroughly with deionized water.

Table 2
Two-sample *t*-test for the PVA coating experiment on S2 microparticles with regard to the pore properties

Property	Plain S2 microparticles				PVA-coated S2 microparticles					
	First replicate	Second replicate	$\bar{y}_{plain}$	S_{plain}	First replicate $q_{e,PVA}$ = 955 mg g^{-1}	Second replicate $q_{e,PVA}$ = 939 mg g^{-1}	$\bar{y}_{with\ PVA}$	$S_{with\ PVA}$	S_p	t_0
S_{BET} ($m^2\,g^{-1}$)	376	365	370	7.4	53	58	56	3.4	5.8	54.4
V_{micro} ($cm^3\,g^{-1}$)	0.05	0.06	0.06	0.011	0.00	0.00	0.00	0.00	0.008	7.2
$V_{10-1000\,Å}$ ($cm^3\,g^{-1}$)	0.97	1.08	1.02	0.079	0.39	0.38	0.38	0.008	0.056	11.4

$t_{\alpha/2, n_{plain}+n_{with\ PVA}-2} = 4.30$.

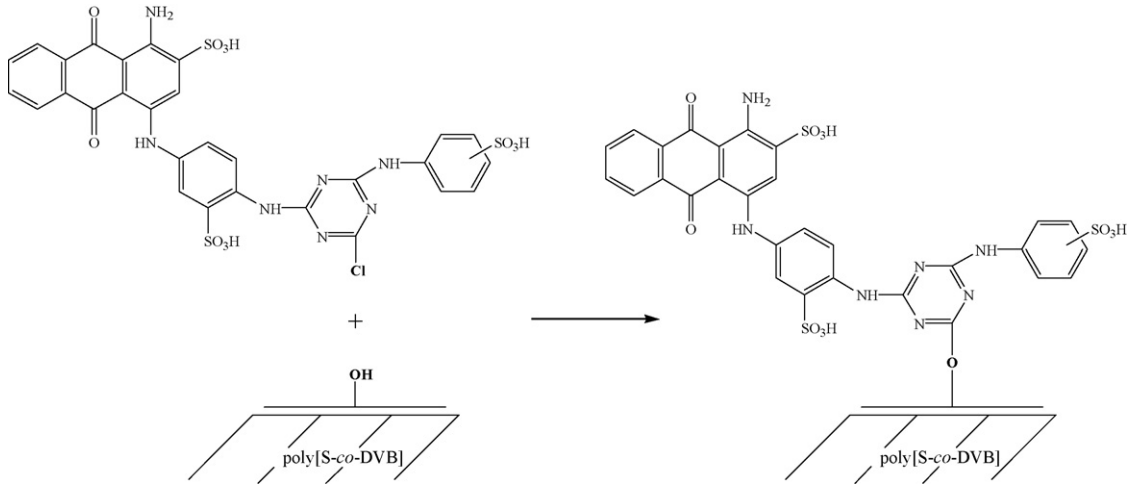

Fig. 1. Chemical structure of Cibacron Blue F3GA and coupling of this ligand to the hydroxyl groups of the PVA coating the poly[S-*co*-DVB] matrix.

To establish the effect of the adsorption of PVA on the structural properties of the microparticles by statistical inference, two plain S2 microparticles and two replicates of adsorption of PVA on these microparticles were obtained (Table 2).

2.2.2. Stabilization of the PVA coating with glutaraldehyde

The PVA molecules adsorbed on the polymeric microparticles were chemically cross-linked to obtain a stable PVA coating on the surface of the microparticles. Glutaraldehyde was used as the cross-linking agent, with a molar ratio for glutaraldehyde to PVA adsorbed of 10:1. A solution of 100 mL of cross-linking agent was poured over 10.0 g of wet PVA-coated poly[S-*co*-DVB] microparticles in a round-bottomed flask. The batch was first stirred mechanically at 50 rpm for 30 min at 30 °C to allow diffusion of the glutaraldehyde into the microparticles. Then, a solution of HCl (5 mol L^{-1}, 0.3 mL) was added to catalyze the cross-linking reaction. The mixture was left at the same temperature for 16 h. Finally, the microparticles were filtered and washed several times with deionized water.

2.2.3. Ligand immobilization

Cibacron Blue F3GA was covalently attached to the PVA-coated poly[S-*co*-DVB] microparticles under alkaline conditions *via* the nucleophilic substitution reaction between the chloride of its triazine ring and the alkoxide anions formed from the hydroxyl groups of the PVA coating (Fig. 1). First, a sample of 10.0 g of microparticles was dispersed in 100 mL of deionized water at 60 rpm and at 60 °C in a round-bottomed flask. Then, 30 mL of a solution of Cibacron Blue F3GA, at a concentration of 33 mg mL^{-1}, was added to the aqueous dispersion. The sample was left to mix well at 60 °C and at 60 rpm in the reactor for 30 min. Then, 15.0 g of NaCl was added to facilitate the interaction between the dye and the matrix [21,22], and the solution was maintained at the same temperature for 45 min. Following this, the medium was heated to 80 °C and 1.5 g of Na_2CO_3 was added to the suspension to obtain the alkaline conditions under which the nucleophilic substitution reaction was performed. The reaction was allowed to progress for 2 h after which the reaction mixture was cooled to room temperature and filtered.

After dye immobilization, in order to remove any uncovalently bound dye, the microparticles were treated with warm water until the washing water was colourless. Finally, microparticles were washed with 1 L of 1.0 mol L^{-1} NaCl, 1 L of 10^{-2} mol L^{-1} $NaHCO_3$ and 1 L of water. The absence of dye leakage was confirmed by spectrophotometry of the supernatant at 610 nm.

The Cibacron Blue F3GA-immobilized microparticles were stored in 0.02% sodium azide at 4 °C to avoid microbial contamination.

2.2.4. Characterization of the polymeric microparticles

The polymeric microparticles were characterized after each modification step. Structural characterization of the microparticles was accomplished using nitrogen adsorption–desorption porosimetry (Micromeritics Gemini V2380 v1.00), which permitted the determination of the BET specific surface area (S_{BET}, m^2 g^{-1}) following the Brunauer–Emmet–Teller method [23], and the micropore volume (V_{micro}, cm^3 g^{-1}) according to the *t*-method [24]. These experimental data were also used to study the pore size distribution of the microparticles, following the Barret–Joyner–Halenda method [25]. The shape of the microparticles was observed with a light microscope (Leica DS1000). Their surface morphology was examined by scanning electron microscopy (SEM), using a Zeiss DSM 940 microscope. UV–Vis spectrophotometry was carried out using a Varian apparatus, model Cary 50.

2.2.5. Protein adsorption–desorption experiments

The usefulness of the functionalized microparticles as adsorbents of proteins was checked *via* a batch method. As mentioned above, chicken egg white lysozyme was selected as a model protein. All pH measurements were performed with a digital pH/mV meter (GLP 21, Crison).

In all experiments, the absence of dye leakage was confirmed by spectrophotometry of the supernatant at 610 nm.

2.2.5.1. Adsorption equilibrium of Lys. Samples of dye-immobilized adsorbent (0.2 g approximately) were weighed and placed in tubes containing 10 mL of a buffer solution (0.05 mol L^{-1} phosphate buffer, pH 7.3) with different, but known, initial concentrations of Lys. The solutions were allowed to equilibrate for 24 h in a rotating shaker, which was placed inside a thermostated chamber to maintain the temperature at 25 °C. After this time, the Lys concentration in the supernatant ($C_{e,Lys}$, mg mL^{-1}) was determined spectrophotometrically at 280 nm. The amount of Lys adsorbed per unit dry weight of adsorbent ($q_{e,Lys}$, mg g^{-1} dry functionalized adsorbent) was obtained from the mass balance given in Eq. (1).

2.2.5.2. Adsorption kinetics of Lys. To study the adsorption kinetics of Lys onto the functionalized microparticles, a buffer solution (0.05 mol L^{-1} phosphate buffer, pH 7.3) with an initial protein con-

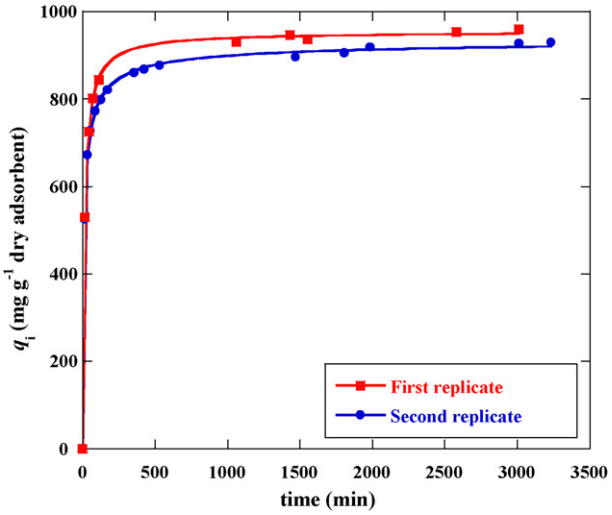

Fig. 2. Adsorption kinetics of PVA onto the S2 sample.

centration of 5 mg mL^{-1} was used. A volume of 100 mL of this solution was poured into a round-bottomed flask that contained 1.5 g of functionalized microparticles. Adsorption proceeded at 25 °C at a stirring speed of 60 rpm. Adsorption kinetic data were obtained by measuring the concentration of Lys in the supernatant spectrophotometrically at 280 nm at different times, which allowed us to determine the amount of Lys adsorbed at these times (q_{ads}, mg g^{-1} dry functionalized adsorbent).

2.2.5.3. Non-specific adsorption of Lys. The effectiveness of the coating in preventing possible non-specific interactions between the protein and the polystyrene support was checked in an experiment involving non-specific protein adsorption. To do so, a sample of 0.2 g of dye-functionalized microparticles was placed in a tube and 10 mL of Lys solution (1 mg mL^{-1} of Lys in 0.05 mol L^{-1} phosphate buffer and 1 mol L^{-1} NaCl, pH 6.7) was added. The sample was left for 24 h in a rotating shaker at 25 °C, after which the Lys concentration in the solution was determined spectrophotometrically at 280 nm. The quantity of protein bound non-specifically ($q_{non\text{-}ads}$, mg g^{-1} functionalized microparticles) was calculated from the mass balance given in Eq. (1).

2.2.5.4. Desorption of Lys. To study the reversibility of protein adsorption on the functionalized microparticles, sodium chloride was used as a desorption agent to decrease the interaction forces between the protein and the adsorbent. Thus, a batch desorption experiment was performed in a phosphate buffer solution of 0.05 mol L^{-1} containing 1 mol L^{-1} NaCl at pH 7.3. In this experiment, Lys-adsorbed microparticles (0.1 g approximately) were placed in the desorption medium and stirred for 24 h at 25 °C. The final Lys concentration in the solution was determined spectrophotometrically at 280 nm. The desorption ratio was calculated as the relationship between the final amount of Lys in the desorption medium and the amount of Lys initially adsorbed on the microparticles.

3. Results and discussion

3.1. PVA adsorption on polymeric microparticles

Fig. 2 shows the adsorption kinetics of PVA onto the poly[S-*co*-DVB] microparticles synthesized with a DVB concentration of 42.5% and a monomeric fraction of 0.50 (S2 sample); it may be observed that PVA adsorption was completed in 6 h. The maximum amount of PVA adsorbed was found to be 267 mg g^{-1} dry adsorbent, on the S1 microparticles; and 947 mg g^{-1} dry adsorbent, on the S2 microparticles (this is the mean value of both replicates, see values in Table 2). The difference in these values can be explained on the basis of the structural properties of the microparticles (Table 1). Essentially, a high specific surface area is due to the presence of micropores and low-interval mesopores, while a high pore volume is due to macropores and high-interval mesopores. Thus, taking into account the higher values of the BET specific surface area and of the micropore volume for the S1 sample, and the higher value of the volume of pores with a radius between 10 Å and 1000 Å for the S2 sample, it may be expected that the S1 sample would have more micropores and low-interval mesopores than S2, while the latter can be presumed to have a higher proportion of high-interval mesopores and macropores, thus admitting a higher amount of PVA. Considering these differences in the porous structure and the high molecular weight of PVA, the existence of steric hindrance can be anticipated to occur during the coating procedure, in such a way that the PVA, instead of penetrating into micropores and low-interval mesopores, simply plugs them at some point along the pore. Consequently, the S1 sample, with smaller pores than those of S2, displays a lower PVA adsorption capacity.

As can be deduced, the study of the structural properties of the microparticles after the adsorption of PVA is essential to obtain an adsorbent with the most appropriate porous structure for a given application. For this reason, it is appropriate to study whether the effect of the adsorption of PVA on the pore properties of the microparticles is statistically significant [26]. To accomplish this, the first step was to obtain the pore properties (S_{BET}, V_{micro} and $V_{10\text{–}1000\,Å}$) of the two replicates of plain S2 microparticles and of the two PVA-coated S2 microparticles. These results are given in Table 2, together with the mean ($\bar{y}$) and the standard deviation of the experimental data (S), and they are plotted in Fig. 3, where the extreme values for each single column are the experimental data, and the mean, which fits in the median, is indicated by lines. From scrutiny of this figure, it may be deduced that the PVA coating influences the pore properties because the S_{BET}, V_{micro} and $V_{10\text{–}1000\,Å}$ decrease notably after PVA adsorption. Nevertheless, to confirm this deduction, a statistical hypothesis testing was performed. The statistical hypothesis may be stated formally as

$$\begin{array}{ll} \text{Null hypothesis} & H_0 : \mu_{plain} = \mu_{with\ PVA} \\ \text{Alternate hypothesis} & H_1 : \mu_{plain} \neq \mu_{with\ PVA} \end{array} \quad (2)$$

where μ_{plain} is the mean pore property of the plain S2 microparticles and $\mu_{with\,PVA}$ is the mean pore property of the PVA-coated S2 microparticles.

To test the hypothesis it is necessary to calculate an appropriate test statistic, thus being able to reject or fail to reject the null hypothesis H_0. Because the sample standard deviations were similar (see values in Table 2), it is not unreasonable to conclude that the population standard deviations (or variances) are equal. Therefore, a two-sample t-test was performed, calculating the t-statistic as follows:

$$t_0 = \frac{\bar{y}_{plain} - \bar{y}_{with\ PVA}}{S_p\sqrt{1/n_{plain} + 1/n_{with\ PVA}}} \quad (3)$$

where $\bar{y}_{plain}$ and $\bar{y}_{with\ PVA}$ are the sample means, and n_{plain} and $n_{with\,PVA}$ are the sample sizes. An estimate of the common variance $\sigma^2_{plain} = \sigma^2_{with\ PVA} = \sigma^2$ is indicated by S_p^2:

$$S_p^2 = \frac{(n_{plain} - 1)S^2_{plain} + (n_{with\ PVA} - 1)S^2_{with\ PVA}}{n_{plain} + n_{with\ PVA} - 2} \quad (4)$$

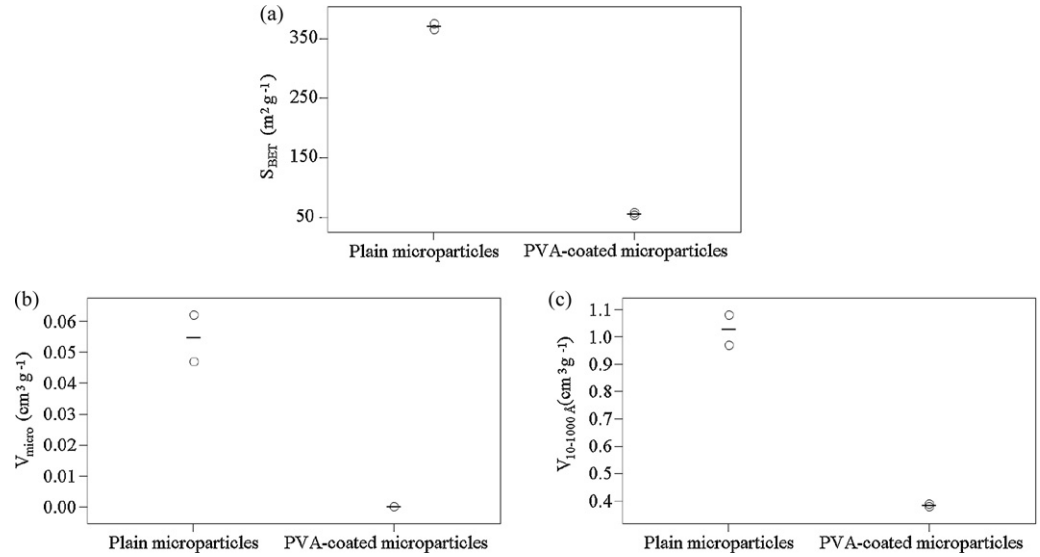

Fig. 3. Dot-plots of the pore properties of S2 microparticles before and after PVA-coating: (a) BET specific surface area ($m^2\ g^{-1}$), (b) volume of micropores ($cm^3\ g^{-1}$), and (c) volume of pores with a pore radius between 10 Å and 1000 Å ($cm^3\ g^{-1}$).

where S^2_{plain} and $S^2_{with\ PVA}$ are the two individual sample variances. The results are given in Table 2.

Since $n_{plain} + n_{with\ PVA} - 2 = 2 + 2 - 2 = 2$, if we choose a significance level of the test of $\alpha = 0.05$, then the null hypothesis, H_0: $\mu_{plain} = \mu_{with\ PVA}$, is rejected because the numerical value of the test statistic, $|t_0|$, is greater than 4.30 for all pore properties ($|t_0| > t_{\alpha/2, n_{plain}+n_{with\ PVA}-2} = 4.30$). This allows us to conclude that the mean pore properties of the S2 microparticles change after the PVA adsorption with a significance level of 0.05.

Other authors have reported the coating of polystyrene matrices with PVA. In this sense, using PVA with a molecular weight of 85,000–146,000 and 99+% hydrolysed and a polymeric matrix with a specific surface area of 200–300 $m^2\ g^{-1}$ (Amberchrom CG162s), Leonard et al. [6] obtained a maximum PVA adsorption of 1.12 $mg\ m^{-2}$ of polystyrene under the best coating conditions. Nevertheless, the PVA saturated the particle surface, producing aggregates of poly[S-*co*-DVB] microparticles. Nash et al. [3] obtained a maximum PVA coating of about 240 $mg\ g^{-1}$ on poly[S-*co*-DVB] microparticles (CG1000sd–TosoHaas) by using PVA with the same molecular weight and degree of hydrolysis as that employed in the present work. Also, Tuncel et al. [7] studied the coating of polystyrene microparticles with PVA (average molecular weight of 14,000, 100% hydrolysed), obtaining a maximum PVA adsorption capacity of 19.0 $mg\ g^{-1}$ of polystyrene under their best experimental conditions; that is, with an initial concentration of 700 $mg\ L^{-1}$ and an ionic strength of 0.2 using sodium sulphate. Shen et al. [10] obtained a maximum PVA adsorption capacity on poly[S-*co*-DVB] microparticles of 247 $mg\ g^{-1}$.

As seen, the different results obtained in these studies are due to the different experimental conditions used during the adsorption process, as well as to the properties of the PVA and of the polystyrene microparticles. Nevertheless, in all cases, the maximum adsorption capacity of PVA on polystyrene microparticles achieved in the present work is higher than those obtained by other authors.

3.2. Nitrogen adsorption–desorption isotherms

Nitrogen adsorption–desorption isotherms were obtained for S1 and S2 samples before and after each modification step, as shown in Fig. 4.

Regarding the plain samples, these nitrogen adsorption–desorption isotherms are of Type II (Fig. 4), according to the IUPAC classification [27], showing that both samples have macropores in their structure. Additionally, the slope and height of the isotherms

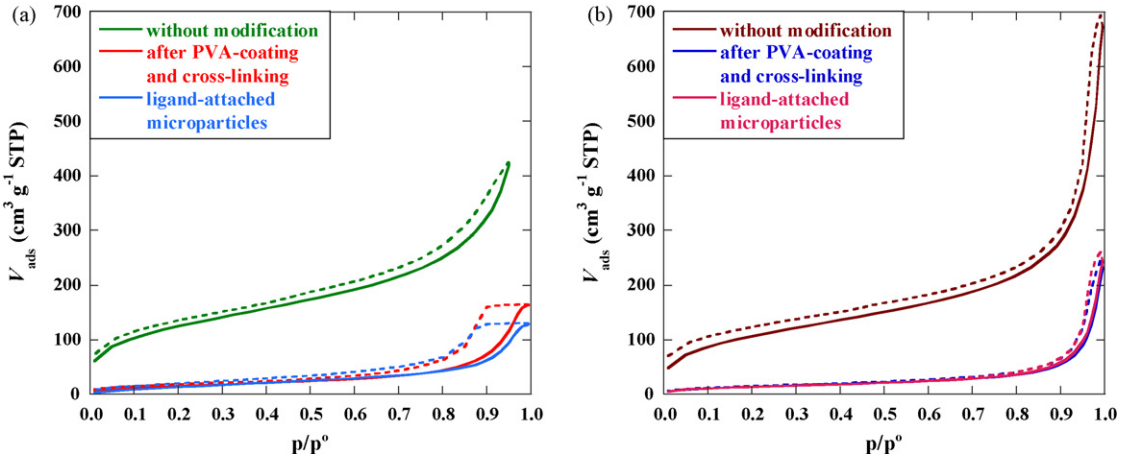

Fig. 4. Nitrogen adsorption–desorption isotherms of microparticles: (a) S1 and (b) S2.

Table 3
Modification of the structural properties of plain microparticles after coating and functionalization

Structural property	Samples					
	S1			S2		
	Plain microparticles	After coating and cross-linking	After function-alization	Plain microparticles	After coating and cross-linking	After functionalization
BET specific surface area ($m^2\ g^{-1}$)	434	58	60	376	51	50
t-Plot micropore volume ($cm^3\ g^{-1}$)	0.06	0.00	0.00	0.05	0.00	0.00
Cumulative volume of pores between 10 Å and 1000 Å radius ($cm^3\ g^{-1}$)	0.81	0.25	0.19	0.97	0.32	0.34
Cumulative surface area of pores between 10 Å and 1000 Å radius ($m^2\ g^{-1}$)	372	68	68	340	56	56
Average pore radius (Å)	44	74	57	57	113	123
Modal pore radius (Å)	244	223	224	284	283	281

in the range of the low relative pressure of nitrogen indicate the presence of micropores, which was confirmed from the values of the micropore volume obtained with the *t*-method [24], as shown in Table 1. Further, high values of the BET specific surface area were obtained.

After the PVA coating of the microparticles and its subsequent cross-linking with glutaraldehyde, the nitrogen adsorption–desorption isotherms changed significantly. Considering first the low-relative pressure range of nitrogen, it can be observed that the micropores disappeared completely from the structure of the microparticles, as confirmed by the values of the micropore volume (Table 3). This was the main reason for the severe decline in the values of the BET specific surface area after the modification of both types of microparticles. With respect to the high-relative pressure range of nitrogen, different kinds of behaviour were observed, depending on the sample. Thus, the PVA-coated microparticles of the S1 sample displayed isotherm of Type IV with a broad hysteresis loop, which indicates that the pores were mainly mesopores subject to difficulties as regards nitrogen desorption as a consequence of their shape. In fact, this is a typical bottle-neck-type hysteresis loop, which corresponds to pores with narrow entrances and wider pores. In contrast, the PVA-coated microparticles of the S2 sample continued to display isotherm of Type II, indicating that the macropores remained in the structure even after the modification.

After the immobilization of Cibacron Blue F3GA on the microparticles, these were analyzed again using the nitrogen adsorption technique. It was observed that, for both samples, the nitrogen adsorption–desorption isotherms did not undergo any significant change. Thus, in both cases, the values of the BET specific surface area were essentially the same before and after the immobilization of the ligand, as seen in Table 3.

3.3. Pore size distributions

From the experimental nitrogen adsorption data, the pore size distributions of both samples were obtained before and after each modification step by following the BJH method [25], as shown in Fig. 5.

For the S1 sample (Fig. 5a), the pore size distribution indicates a high proportion of mesopores in the structure of the microparticles. In contrast, the presence of macropores was less patent and, moreover, they decreased abruptly from a pore radius of 400 Å. After being PVA-coated and cross-linked with glutaraldehyde, the micropores were almost completely clogged, and the size and quantity of pores with a pore radius between 10 Å and 70 Å decreased considerably. Regarding the macropores, although the modal pore radius

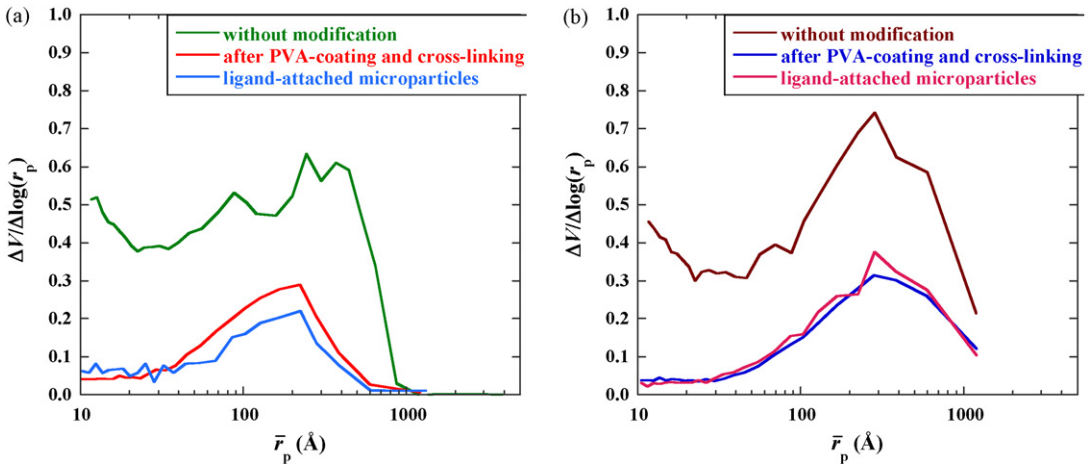

Fig. 5. Pore size distributions of microparticles: (a) S1 and (b) S2. *Note*: the experimental data on the adsorption of nitrogen by the plain S1 microparticles have been completed with mercury porosimetry data to obtain the complete pore size distribution.

remained almost unchanged (see values in Table 3), the size and the quantity of macropores decreased abruptly from the modal pore radius. Nevertheless, the average pore radius increased because the decrease in pore volume was not so rapid as the decrease in pore surface (Table 3). Regarding the immobilization of the ligand to the microparticles, no significant changes can be appreciated in the pore size distribution of this sample of microparticles.

Considering the S2 sample (Fig. 5b), the pore size distribution shows a modal form, with a maximum value at 284 Å. After being PVA-coated and cross-linked, and also after immobilization, the microparticles continued to have the same modal pore radius but, as in the case of microparticles of the S1 sample, the average pore radius increased significantly (see values in Table 3). Regarding the macropores, although their quantity decreased after functionalization, this was not as abrupt as for the S1 sample.

3.4. Lysozyme adsorption equilibrium

Experiments addressing the lysozyme adsorption equilibrium on both functionalized samples were performed. However, in the case of the use of the S1 sample as an adsorbent, no appreciable adsorption was obtained. This can be explained in terms of the desorption branch of its nitrogen isotherm in Fig. 4a, where it can be observed that this branch is almost horizontal over the range from $p/p^0 = 0.900$ to $p/p^0 = 0.995$ of nitrogen uptake, before which there is a sharp decrease. The value of the pore radius corresponding to this sharp decrease is about 75 Å meaning that, although the microparticles display the pore size distribution shown in Fig. 5a, access to these pores is limited by narrower necks, with radii of about 75 Å. Therefore, this complicates the penetration of the protein to the adsorption sites.

Considering the functionalized S2 adsorbent, Lys adsorption equilibrium data on this adsorbent were obtained, as shown in Fig. 6. Different adsorption models (Langmuir, Freundlich, double Langmuir, Sips, Toth, etc.) were fitted to these adsorption equilibrium data. The Langmuir and Freundlich models can be expressed as follows:

$$\text{Langmuir model} \quad q_e = \frac{q_m b C_e}{1 + b C_e} \tag{5}$$

$$\text{Freundlich model} \quad q_e = A C_e^{1/n} \tag{6}$$

where q_m (mg g^{-1} dry functionalized adsorbent) is the maximum adsorption capacity of Lys on the adsorption sites; b (mL mg^{-1}) is a parameter related to the affinity between the adsorbate and the adsorption sites; A is a coefficient indicative of the relative adsorption capacity of the adsorbent; n is a parameter related to the adsorption intensity.

In the Langmuir isotherm (Eq. (5)), the value of the b parameter depends on the energy of adsorption and it is assumed that this value is the same for each active site and is independent of the presence of nearby adsorbed molecules. However, in the case of the adsorption of proteins, the protein–ligand interactions are often very complex and it is frequently found that the Langmuir model is unable to adequately explain the shape of the experimental equilibrium isotherm.

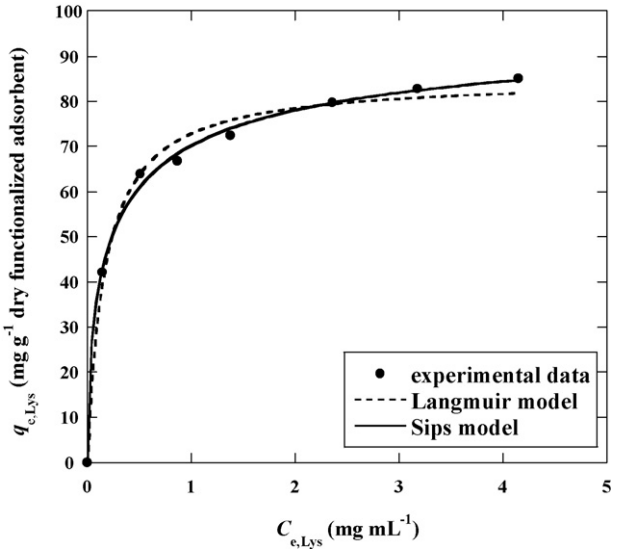

Fig. 6. Curve of the adsorption isotherm of Lys on the Cibacron Blue F3GA-immobilized polymeric microparticles of the S2 sample.

The Freundlich isotherm (Eq. (6)) is more flexible and assumes that the energy of adsorption decreases logarithmically as the fractional coverage increases. However, the Freundlich isotherm does not tend to a limiting coverage as the concentration tends to infinity. Additionally, Sips [28] proposed a model (Eq. (7)) that is a combination of Langmuir and Freundlich models and that eludes this limitation.

$$q_e = \frac{q_m b C_e^{1/n}}{1 + b C_e^{1/n}} \tag{7}$$

The underlying assumption in the Sips model is the existence of adsorption sites in such a way that the energy of the diverse types of possible interactions between the adsorbate and the adsorbent can be described by a symmetrical, quasi-Gaussian, energy distribution curve. This assumption seems to be very appropriate in the case of affinity adsorption because of the diverse types of binding that can occur between the adsorbate and the adsorbent.

The fitting of the models to the adsorption equilibrium data was accomplished by multiple non-linear regression techniques. The Langmuir (Eq. (5)) and Sips (Eq. (7)) models emerged as the

Table 4
Adsorption properties of the functionalized macroreticular poly(styrene-*co*-divinylbenzene) microparticles of the S2 sample

Adsorption properties	Value				
	q_m (mg g^{-1} dry functionalized adsorbent)	b (mL mg^{-1})	n	χ^2	R^2
Lys adsorption equilibrium					
Langmuir model	85.1 ± 2.0	5.9 ± 0.8	1	53.0	0.991
Sips model	100.8 ± 7.7	2.3 ± 0.6	1.7 ± 0.3	13.1	0.998

Adsorption properties	Value	
	D_i ($\times 10^{-9}$ cm^2 s^{-1})	R^2
Lys adsorption kinetics		
Shrinking-core model	4.0	0.943
Simplified solid-diffusion model	1.4	0.989

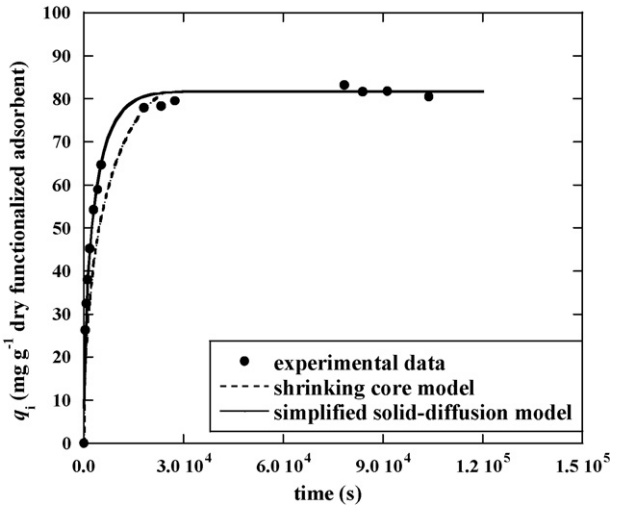

Fig. 7. Curve of the adsorption kinetics of Lys onto the Cibacron Blue F3GA-immobilized polymeric microparticles of the S2 sample.

best models to describe the adsorption phenomenon. The calculated values of the parameters of these equations as well as the chi-square value (χ^2) and the coefficient of determination (R^2) are given in Table 4. The curves resulting from these fits are plotted in Fig. 6. It may be observed that the best results were obtained when the Sips model was used. This is also corroborated by the values of χ^2 and R^2, because the lower the value of χ^2 and the closer to unity the value of R^2, the better the fit.

As deduced from data in Table 4, the maximum adsorption capacity of Lys on the functionalized S2 adsorbent is 100.8 mg g^{-1}.

3.5. Lysozyme adsorption kinetics

Kinetic data concerning the adsorption of Lys onto the functionalized S2 adsorbent were obtained at different times, as shown in Fig. 7, where q_i is plotted versus time. It may be considered that usually there are three steps involved in protein adsorption from a bulk solution onto a solid adsorbent, all of which can be considered to offer resistance to protein uptake. These steps include mass transfer from the bulk liquid to the outer surface of the particles (external mass transfer resistance), movement of the adsorbent into the pores by diffusion (internal mass transfer resistance), and protein binding to the ligand (adsorption resistance). The global uptake rate can be controlled by one or more of these three types of resistance, depending on the type of adsorbent and adsorbate and also on the operating conditions employed during the uptake process. Usually, in protein uptake processes, steps 1 and 2 are rate-limiting, because such processes have a tendency to take place much slower than adsorption.

Two models are commonly used to characterize the transport of proteins in porous particles [29,30], each involving a different driving force: (1) the pore-diffusion model and (2) the solid-diffusion model.

In the pore-diffusion model, protein diffusion is assumed to be governed by the protein concentration gradient in the liquid-filled pores, accompanied by adsorption onto the bounding pore walls. This behaviour is described by the following equation:

$$\left[\varepsilon_p + (1-\varepsilon_p)\frac{\partial q'}{\partial c}\right]\frac{\partial c}{\partial t} = \frac{D_e}{r^2}\frac{\partial}{\partial r}\left(r^2\frac{\partial c}{\partial r}\right) \tag{8}$$

where c and q', that is, the concentration of protein in the pores (mg mL^{-1}) and in the particles on a pore-free basis (mg mL^{-1}), respectively, are expressed as functions of the radial position r (cm) and uptake time t (s). D_e is the effective pore diffusivity (cm^2 s^{-1}), and ε_p is the intraparticle porosity of the adsorbent. When the adsorption isotherm is non-linear, a numerical solution is generally required. However, for a rectangular adsorption isotherm [31], the adsorption front within the particle approaches a shock transition, separating an inner core into which the adsorbate has not yet penetrated from an outer layer in which the adsorbed phase concentration is uniform at the saturation value. The dynamics of this process can be described approximately by the shrinking-core model. Under our experimental conditions, that is (i) external film resistance negligible as a consequence of the high initial protein concentration and (ii) finite volume conditions due to the decrease in the protein concentration in the bulk solution as adsorption takes place, this model can be written as follows [32]:

$$\frac{D_e C_0}{R_p^2 q_m^*}t = I_2 - I_1 \tag{9}$$

where and I_1 and I_2 are given by

$$I_1 = \frac{1}{6\lambda\Lambda}\ln\left[\frac{\lambda^3+\eta^3}{\lambda^3+1}\left(\frac{\lambda+1}{\lambda+\eta}\right)^3\right] + \frac{1}{\lambda\Lambda\sqrt{3}}\left[\tan^{-1}\left(\frac{2\eta-\lambda}{\lambda\sqrt{3}}\right) - \tan^{-1}\left(\frac{2-\lambda}{\lambda\sqrt{3}}\right)\right] \tag{10}$$

$$I_2 = \frac{1}{3\Lambda}\ln\left[\frac{\lambda^3+\eta^3}{\lambda^3+1}\right] \tag{11}$$

with

$$\eta = \left(1 - \frac{\bar{q}^*}{q_m^*}\right)^{1/3} \tag{12}$$

$$\Lambda = \frac{V_M q_m^*}{V C_0} \tag{13}$$

$$\lambda = \left(\frac{1}{\Lambda} - 1\right)^{1/3} \tag{14}$$

where $\bar{q}^*$ is the particle-average solute concentration (mg mL^{-1}), q_m^* is the maximum solute adsorption capacity in the particles (mg mL^{-1}), V_M is the volume of microparticles (mL), and V is the bulk solution volume (mL).

Application of the shrinking-core model (Eq. (9)) to the experimental kinetic data allowed us to determine the effective pore diffusivity ($D_e = 4.0 \times 10^{-9}$ cm^2 s^{-1}) and the theoretical kinetic curve, which is plotted in Fig. 7 together with the experimental data. It can be seen that this model represents the experimental behaviour in the saturation zone correctly, but that it does not allow the beginning of the curve to be fitted. Accordingly, the pore-diffusion model was discarded and the solid-diffusion model was investigated.

In the solid-diffusion model, all the protein inside the particle is assumed to be free to diffuse, the flux being based on the gradient in the total protein concentration [33]. This behaviour is described by the following equation [34]:

$$\frac{\partial q}{\partial t} = \frac{D_s}{r^2}\frac{\partial}{\partial r}\left(r^2\frac{\partial q}{\partial r}\right) \tag{15}$$

where D_s is the solid-diffusion coefficient (cm^2 s^{-1}). In general, a numerical solution of the model is required. However, for modelling batch uptake from a finite fluid volume when the external mass transfer resistance is negligible, an approximation to this numerical solution can be used:

$$\frac{q_{ads}}{q_m} = 1 - 6\sum_{n=1}^{\infty}\frac{\exp(-D_s p_n^2 t/R_p^2)}{9\Lambda/(1-\Lambda) + (1-\Lambda)p_n^2} \tag{16}$$

where p_n is given by the positive roots of

$$\tan p_n = \frac{3p_n}{3 + (1/\Lambda - 1)p_n^2} \quad (17)$$

By applying Eq. (16) to the experimental kinetic data, the solid-diffusion coefficient was determined ($D_s = 1.4 \times 10^{-9}$ cm^2 s^{-1}), allowing us to obtain the theoretical kinetic curve and to compare it with the experimental data (Fig. 7). It can be observed that the simplified solid-diffusion model given by Eq. (16) fits the data satisfactorily across the entire time range considered.

With regard to the values of the diffusion models obtained with both models (Eqs. (9) and (16)), it can be seen that the solid-diffusion coefficient, D_s, is smaller than the pore-diffusion coefficient, D_e. In fact, D_s is typically smaller than D_e for a given system because of the concentrating effect of adsorption: locally, q is generally higher than c, and the gradient $\partial q/\partial r$ is correspondingly higher than $\partial c/\partial r$ [33].

Comparison of the results obtained here with those obtained in other studies addressing Lys adsorption equilibrium and kinetics using Cibacron Blue F3GA-attached affinity supports is very difficult because, in most cases, either only the adsorption equilibrium results are given [13,16,35,36] or the procedures used to obtain and analyze the experimental data are not the same as those employed in this work [3–5,15,37]. For example, some authors have analyzed data on adsorption kinetics by applying pseudo-first-order and pseudo-second-order kinetic models instead of using diffusion models [38]. However, Xue and Sun [39] reported some results that can be compared with those obtained by us. Those authors synthesized Cibacron Blue F3GA-attached PVA microparticles containing Fe_3O_4 colloidal particles, with a mean particle size of 42.6 μm and a density of 1.12 g mL^{-1} calculated with the voidage and density of packed bed, and used them as adsorbents for Lys adsorption. They found that, under their best experimental conditions, the maximum Lys adsorption capacity was 254 mg mL^{-1}, with a value of 8.0×10^{-8} cm^2 s^{-1} for D_e and a value of 6.0×10^{-11} cm^2 s^{-1} for D_s.

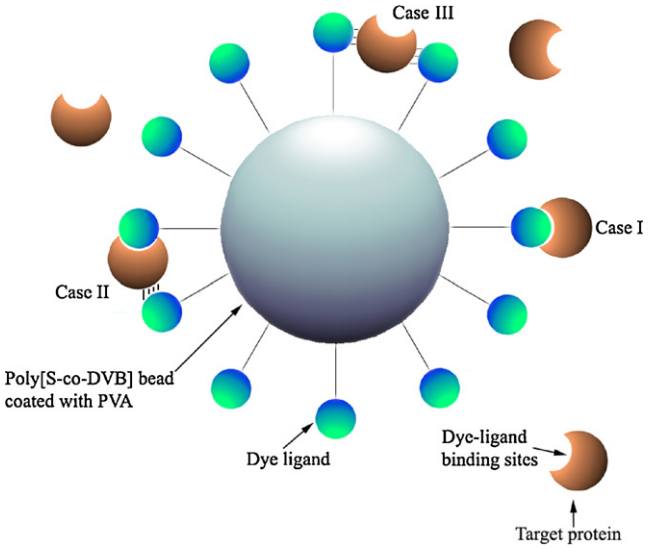

Fig. 8. Schematic representation of some of the possible interactions between the protein and the dye–ligand attached to the PVA coating the polymeric surface: specific interaction (case I), specific and non-specific interaction (case II), and non-specific interaction (case III).

3.6. Non-specific lysozyme adsorption

The effectiveness of the hydrophilic functionalization achieved by PVA coating and subsequent immobilization of Cibacron Blue F3GA in preventing possible non-specific interactions between the polymeric matrix and the protein was established by determining non-specific Lys adsorption. A scheme representation of some of the possible specific and non-specific interactions between the protein and the adsorbent is shown in Fig. 8.

As already reported, this experiment was performed *via* a batch method, by measuring the amount of Lys bound to the functionalized microparticles in the presence of a solution of Lys (1 mg mL^{-1})

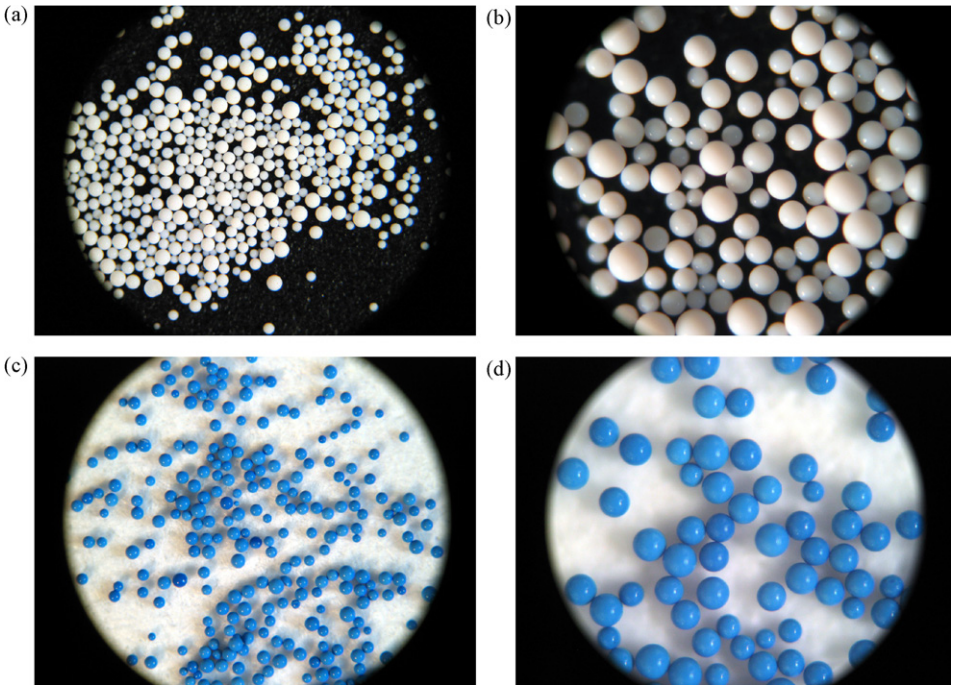

Fig. 9. Light microscopy photographs showing the modification of the S2 plain polymeric microparticles (a and b) after the immobilization of Cibacron Blue F3GA (c and d). Mean particle size is 170 μm.

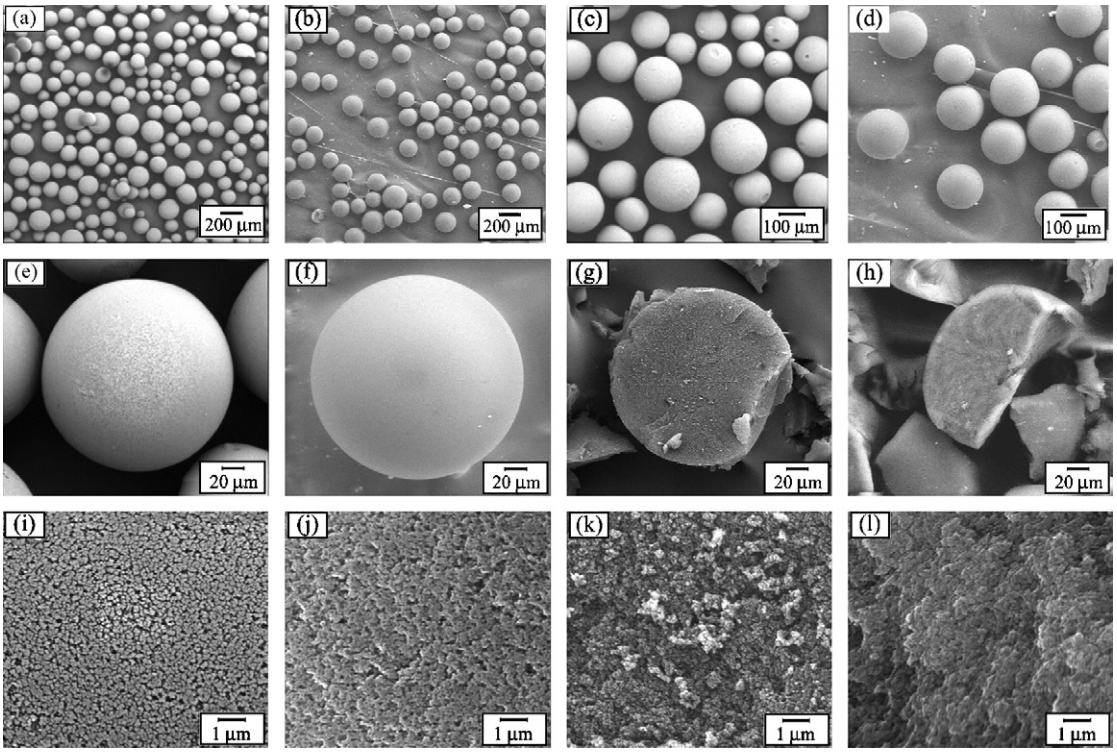

Fig. 10. Scanning electron microscopy photographs showing the modification of the S2 microparticles after attachment of the ligand. Photographs of the plain microparticles are given in a, c, e, g, i and k. Photographs of the Cibacron Blue F3GA-attached polymeric microparticles are given in b, d, f, h, j and l.

of high ionic strength (1 mol L^{-1} NaCl in 0.05 mol L^{-1} phosphate buffer, pH 6.7). It was observed that only 2.6 mg of protein per gram of dry functionalized adsorbent was adsorbed. Taking this result into account, it may be concluded that functionalization was achieved in a satisfactory manner.

3.7. Desorption of lysozyme

An adsorbent is useful if recovery of the protein adsorbed is possible. Accordingly, a desorption experiment was carried out using a batch method. In this experiment, Lys-adsorbed microparticles were placed in tubes with a solution of high ionic strength (1 mol L^{-1} NaCl in 0.05 mol L^{-1} phosphate buffer, pH 7.3). The results showed that 73% of the Lys adsorbed was desorbed when NaCl was used as the desorption agent. The desorption of Lys is assumed to be due to the fact that NaCl decreases the specific interactions between the positively charged groups of Lys and the negatively charged dye.

3.8. Light and scanning electron microscopy

Microparticles of the S2 sample were characterized by light microscopy before and after functionalization, as shown in Fig. 9. The colour modification of the microparticles after covalent incorporation of the ligand may be observed. The images also show that, despite the high amount of PVA adsorbed (955 mg g^{-1} dry adsorbent), the microparticles continue to be non-agglomerated, with a perfectly spherical form.

Additionally, SEM photographs of the plain and ligand-attached microparticles of the S2 sample were obtained, as seen in Fig. 10. The detailed surface morphology of the microparticles reveals the coating with PVA. It can also be seen that macropores remained after the attachment of the ligand to the microparticles.

4. Conclusions

Hydrophilic adsorbents suitable for the adsorption of biomolecules have been obtained by the modification of macroreticular poly[S-*co*-DVB] microparticles with different pore properties. To accomplish this, in a first step a PVA coating procedure was carried out to shield the surface of the polymeric microparticles, thereby ensuring minimal non-specific biomolecule adsorption. The PVA adsorption layer was later cross-linked with glutaraldehyde to provide a chemically stable coating and, finally, the microparticles were functionalized with the triazine dye Cibacron Blue F3GA.

Structural changes in the microparticles were studied after each modification step. Thus, with regard to the coating with PVA, both micropores and low-interval mesopores were clogged, and hence very low values of the BET specific surface area were obtained. Regarding high-interval mesopores and macropores, these only remained in the structure of the microparticles which, initially, displayed a higher pore volume. Considering the immobilization of the ligand, no significant change was observed.

The adsorption properties of the dye-immobilized adsorbents were tested using lysozyme as a model protein. It was found that the adsorption of Lys was only possible on microparticles that largely continued to exhibit high-interval mesopores and macropores after functionalization. For these microparticles, it was seen that the adsorption of Lys obeyed the Sips model, with a maximum adsorption capacity of 100.8 mg g^{-1} dry functionalized adsorbent. Also, the adsorption kinetics of Lys onto these microparticles was studied with two simplified diffusion models, that is, the shrinking-core model and the simplified solid-diffusion model. The results revealed that the latter model fitted the experimental data satisfactorily across the entire time range studied, with a solid-diffusion coefficient of 1.4×10^{-9} cm^2 s^{-1}.

The non-specific adsorption of Lys on the dye-immobilized microparticles was also studied in a batch system and it was found to be 2.6 mg of protein per gram of functionalized adsorbent. Additionally, a high desorption ratio (over 73% of the Lys adsorbed) was obtained by using a 1 mol L^{-1} NaCl solution in a batch process.

Acknowledgements

This work was supported financially by the Spanish Ministry of Science and Technology (CTQ2006-13709), the Educational Council of the Junta de Castilla y León (SA039A07), and the European Social Fund.

References

[1] S.R. Narayanan, Preparative affinity chromatography of proteins, J. Chromatogr. A 658 (2) (1994) 237–258.
[2] J. Carlsson, J.C. Janson, M. Sparrman, Affinity chromatography, in: J.C. Janson, L. Ryden (Eds.), Protein Purification: Principles, High Resolution Methods, and Applications, Wiley-VCH, New York, 1989.
[3] D.C. Nash, G.E. McCreath, H.A. Chase, Modification of polystyrenic matrices for the purification of proteins. Effect of the adsorption of poly(vinyl alcohol) on the characteristics of poly(styrene-divinylbenzene) beads for use in affinity chromatography, J. Chromatogr. A 758 (1) (1997) 53–64.
[4] D.C. Nash, H.A. Chase, Modification of polystyrenic matrices for the purification of proteins. II. Effect of the degree of glutaraldehyde–poly(vinyl alcohol) crosslinking on various dye ligand chromatography systems, J. Chromatogr. A 776 (1) (1997) 55–63.
[5] D.C. Nash, H.A. Chase, Modification of polystyrenic matrices for the purification of proteins. III. Effects of poly(vinyl alcohol) modification on the characteristics of protein adsorption on conventional and perfusion polystyrenic matrices, J. Chromatogr. A 776 (1) (1997) 65–73.
[6] M. Leonard, C. Fourier, E. Dellacherie, Polyvinyl alcohol-coated macroporous polystyrene particles as stationary phases for the chromatography of proteins, J. Chromatogr. B 664 (1) (1995) 39–46.
[7] A. Tuncel, A. Denizli, D. Purvis, C.R. Lowe, E. Piskin, Cibacron Blue F3G-A-attached monosize poly(vinyl alcohol)-coated polystyrene microspheres for specific albumin adsorption, J. Chromatogr. A 634 (2) (1993) 161–168.
[8] L. Varady, N. Mu, Y.B. Yang, S.E. Cook, N. Afeyan, F.E. Regnier, Fimbriated stationary phases for proteins, J. Chromatogr. A 631 (1–2) (1993) 107–114.
[9] Y.B. Yang, F.E. Regnier, Coated hydrophilic polystyrene-based packing materials, J. Chromatogr. A 544 (1991) 233–247.
[10] L. Shen, B.H. Xiong, R.Z. Cong, J.D. Wang, Preparation of Cibacron Blue F3GA bonded poly(styrene-divinylbenzene) (PSDVB) microbeads used for high performance affinity chromatography, Chin. Chem. Lett. 10 (7) (1999) 583–586.
[11] K. Hosoya, Y. Kishii, K. Kimata, T. Araki, N. Tanaka, F. Svec, J.M.J. Frechet, Uniform-size hydrophobic polymer-based separation media selectively modified with a hydrophilic external polymeric layer, J. Chromatogr. A 690 (1) (1995) 21–28.
[12] G. Bayramoglu, F.B. Senkal, G. Celik, M.Y. Arica, Preparation and characterization of sulfonyl-hydrazine attached poly(styrene-divinylbenzene) beads for separation of albumin, Colloid Surf. A: Physicochem. Eng. Asp. 294 (1–3) (2007) 56–63.
[13] N. Basar, L. Uzun, A. Güner, A. Denizli, Lysozyme purification with dye-affinity beads under magnetic field, Int. J. Biol. Macromol. 41 (3) (2007) 234–242.
[14] T. Atkinson, P.M. Hammond, R.D. Hartwell, P. Hughes, M.D. Scawen, R.F. Sherwood, D.A.P. Small, C.J. Bruton, M.J. Harvey, C.R. Lowe, Triazine dye affinity chromatography, Biochem. Soc. Trans. 9 (4) (1981) 290–293.
[15] M.Y. Arica, G. Bayramoglu, Purification of lysozyme from egg white by Reactive Blue 4 and Reactive Red 120 dye–ligands immobilised composite membranes, Process Biochem. 40 (3–4) (2005) 1433–1442.
[16] E. Unsal, A. Durdu, B. Elmas, M. Tuncel, A. Tuncel, A new affinity-HPLC packing for protein separation: Cibacron blue attached uniform porous poly(HEMA-*co*-EDM) beads, Anal. Bioanal. Chem. 383 (6) (2005) 930–937.
[17] A. Denizli, E. Piskin, Dye–ligand affinity systems, J. Biochem. Biophys. Methods 49 (1–3) (2001) 391–416.
[18] C. Garcia-Diego, J. Cuellar, Synthesis of macroporous poly(styrene-*co*-divinylbenzene) microparticles using *n*-heptane as the porogen: quantitative effects of the DVB concentration and the monomeric fraction on their structural characteristics, Ind. Eng. Chem. Res. 44 (22) (2005) 8237–8247.
[19] C. Garcia-Diego, J. Cuellar, Determination of the quantitative relationships between the synthesis conditions of macroporous poly(styrene-*co*-divinylbenzene) microparticles and the characteristics of their behavior as adsorbents using bovine serum albumin as a model macromolecule, Ind. Eng. Chem. Res. 45 (10) (2006) 3624–3632.
[20] C. Garcia-Diego, J. Cuellar, Application of cluster analysis and optimization to determine the synthesis conditions of macroreticular poly(styrene-*co*-divinylbenzene) microparticles with enhanced structural and adsorption properties, Chem. Eng. J. 139 (1) (2008) 198–207.
[21] P.D.G. Dean, D.H. Watson, Protein purification using immobilized triazine dyes, J. Chromatogr. A 165 (3) (1979) 301–319.
[22] S. Zhang, Y. Sun, Further studies on the contribution of electrostatic and hydrophobic interactions to protein adsorption on dye–ligand adsorbents, Biotechnol. Bioeng. 75 (6) (2001) 710–717.
[23] S. Brunauer, P.H. Emmet, E. Teller, Adsorption of gases in multimolecular layers, J. Am. Chem. Soc. 60 (1938) 309–319.
[24] B.C. Lippens, J.H. de Boer, Studies on pore systems in catalysts. V. *t* method, J. Catal. 4 (3) (1965) 319–323.
[25] E.P. Barrett, L.G. Joyner, P.P. Halenda, The determination of pore volume and area distributions in porous substances. I. Computations from nitrogen isotherms, J. Am. Chem. Soc. 73 (1) (1951) 373–380.
[26] D.C. Montgomery, Design and Analysis of Experiments, 5th ed., John Wiley & Sons, New York, 2001, pp. 33–36.
[27] K.S.W. Sing, D.H. Everett, R.A.W. Haul, L. Moscou, R.A. Pierotti, J. Rouquerol, T. Siemieniewska, Reporting physisorption data for gas/solid systems with special reference to the determination of surface area and porosity (recommendations 1984), Pure Appl. Chem. 57 (4) (1985) 603–619.
[28] R. Sips, On the structure of a catalyst surface, J. Chem. Phys. 16 (5) (1948) 490–495.
[29] D.M. Ruthven, Principles of Adsorption and Adsorption Processes, Wiley, New York, 1984.
[30] L.E. Weaver, G. Carta, Protein adsorption on cation exchangers: comparison of macroporous and gel-composite media, Biotechnol. Prog. 12 (3) (1996) 342–355.
[31] A.K. Hunter, G. Carta, Protein adsorption on novel acrylamido-based polymeric ion exchangers. II. Adsorption rates and column behaviour, J. Chromatogr. A 897 (1–2) (2000) 81–97.
[32] W.K. Teo, D.M. Ruthven, Adsorption of water from aqueous ethanol using 3-Å molecular sieves, Ind. Eng. Chem. Process Des. Dev. 25 (1) (1986) 17–21.
[33] C. Chang, A.M. Lenhoff, Comparison of protein adsorption isotherms and uptake rates in preparative cation-exchange materials, J. Chromatogr. A 827 (2) (1998) 281–293.
[34] J. Crank, The Mathematics of Diffusion, 2nd ed., Oxford University Press, London, 1975.
[35] S. Senel, R. Say, Y. Arica, A. Denizli, Zinc ion-promoted adsorption of lysozyme to Cibacron Blue F3GA-attached microporous polyamide hollow-fiber membranes, Colloid Surf. A: Physicochem. Eng. Asp. 182 (1–3) (2001) 161–173.
[36] M. Odabasi, A. Denizli, Cibacron Blue F3GA incorporated magnetic poly(2-hydroxyethyl methacrylate) beads for lysozyme adsorption, J. Appl. Polym. Sci. 93 (2) (2004) 719–725.
[37] A. Denizli, S. Senel, M.Y. Arica, Cibacron Blue F3GA and Cu(II) derived poly(2-hydroxyethylmethacrylate) membranes for lysozyme adsorption, Colloid Surf. B: Biointerfaces 11 (3) (1998) 113–122.
[38] E.B. Altintas, A. Denizli, Monosize poly(glycidyl methacrylate) beads for dye-affinity purification of lysozyme, Int. J. Biol. Macromol. 38 (2) (2006) 99–106.
[39] B. Xue, Y. Sun, Protein adsorption equilibria and kinetics to a poly(vinyl alcohol)-based magnetic affinity support, J. Chromatogr. A 921 (2) (2001) 109–119.